Bacterial Metabolites and Particle Size Determine Cerium Oxide Nanomaterial Biotransformation

Blanche Collin, Mélanie F Auffan, Emmanuel Doelsch, Olivier Proux, Isabelle Kieffer, Philippe Ortet, Catherine Santaella

Bacterial metabolites and particle size determine cerium oxide nanomaterial biotransformation

Journal:	*Environmental Science & Technology*
Manuscript ID	es-2022-05280z.R1
Manuscript Type:	Article
Date Submitted by the Author:	13-Sep-2022
Complete List of Authors:	Collin, Blanche; CEREGE, environnement durable Auffan, Melanie; CNRS, CEREGE Doelsch, Emmanuel; CIRAD, Environmental Risks of Recycling Research Unit Proux, Olivier; European Synchrotron Radiation Facility Kieffer, Isabelle; ESRF, BM30B/Fame beamline Ortet, Philippe; CEA, IBEB, Lab Ecol Microb Rhizosphere & Environ Extrem, Environmental Biology Santaella, Catherine; Aix-Marseille-University, CEA, CNRS, BIAM, LEMIRE

Bacterial metabolites and particle size determine cerium oxide nanomaterial biotransformation

Blanche Collin[1,2*], Mélanie Auffan[1], Emmanuel Doelsch[3,4], Olivier Proux[5], Isabelle Kieffer[5], Philippe Ortet[2], Catherine Santaella[2*]

1: Aix Marseille Univ, CNRS, IRD, INRAE, Coll France, CEREGE, Aix-en-Provence, France
2: Aix Marseille Univ, CEA, CNRS, BIAM, LEMIRE, Laboratory of Microbial Ecology of the Rhizosphere, ECCOREV FR 3098, F-13108, St-Paul-lez-Durance, France
3: CIRAD, UPR Recyclage et risque, F-34398 Montpellier, France
4: Recyclage et risque, Univ Montpellier, CIRAD, Montpellier, France
5: BM30/CRG-FAME, ESRF, Université Grenoble Alpes, CNRS, IRSTEa, Météo France, IRD, OSUG, Grenoble 38000, France

***Corresponding Authors:**

Blanche Collin
Aix Marseille Univ, CNRS, IRD, INRAE, Coll France, CEREGE, Aix-en-Provence, France
Aix Marseille Univ, CEA, CNRS, BIAM, LEMIRE, Laboratory of Microbial Ecology of the Rhizosphere, ECCOREV FR 3098, F-13108, St-Paul-lez-Durance, France
collin@cerege.fr

Catherine Santaella
Aix Marseille Univ, CEA, CNRS, BIAM, LEMIRE, Laboratory of Microbial Ecology of the Rhizosphere, ECCOREV FR 3098, F-13108, St-Paul-lez-Durance, France
catherine.santaella@cea.fr

Authors:

Mélanie Auffan
Aix Marseille Univ, CNRS, IRD, INRAE, Coll France, CEREGE, Aix-en-Provence, France

Emmanuel Doelsch
CIRAD, UPR Recyclage et risque, F-34398 Montpellier, France
Recyclage et risque, Univ Montpellier, CIRAD, Montpellier, France

Olivier Proux
BM30/CRG-FAME, ESRF, Université Grenoble Alpes, CNRS, IRSTEa, Météo France, IRD, OSUG, Grenoble 38000, France

Isabelle Kieffer

BM30/CRG-FAME, ESRF, Université Grenoble Alpes, CNRS, IRSTEa, Météo France, IRD, OSUG, Grenoble 38000, France

Philippe Ortet
Aix Marseille Univ, CEA, CNRS, BIAM, LEMIRE, Laboratory of Microbial Ecology of the Rhizosphere, ECCOREV FR 3098, F-13108, St-Paul-lez-Durance, France

Abstract

Soil is a major receptor of manufactured nanomaterials (NMs) following unintentional releases or intentional uses. Ceria NMs have been shown to undergo biotransformation in plant and soil organisms with a partial Ce(IV) reduction into Ce(III) but the influence of environmentally widespread soil bacteria is poorly understood. We used high-energy resolution fluorescence detected X-ray absorption spectroscopy (HERFD-XAS) with an unprecedented detection limit to assess Ce speciation in a model soil bacterium (*Pseudomonas brassicacearum*) exposed to CeO_2 NMs of different sizes and shapes. The findings revealed that the CeO_2 NMs size drives the biotransformation process. No biotransformation was observed for the 31 nm CeO_2 NMs, contrary to 7 nm and 4 nm CeO_2 NMs, with a Ce reduction of 64 ± 14% and 70 ± 15%, respectively. This major reduction appeared quickly, from the early exponential bacterial growth phase. Environmentally relevant organic acid metabolites secreted by *Pseudomonas*, especially in the rhizosphere, were investigated. The 2-keto-gluconic and citric acid metabolites alone were able to induce a significant reduction in 4 nm CeO_2 NMs. The high biotransformation measured for < 7 nm NMs would affect the fate of Ce in the soil and biota.

Synopsis

Soil bacteria are widespread in the environment but little is known on their influence on the fate of nanomaterials. The NM size, the bacterial interaction and bacterial metabolites drive NM bioreduction.

Introduction

The biological transformation of nanomaterials (NMs) is a key to understanding the impact and fate of NMs in the environment.[1, 2] Soil is a major environmental collector for NMs, along with sediment and landfill.[3, 4] Soil is also a complex ecological system hosting a diverse range of living organisms and millions of microorganisms that can induce environmental NM transformation at the scale of the organisms, tissues, cells and biomolecules. Plants and microorganisms secrete secondary metabolites, i.e. specialized molecules, that are essential for their biological activities while modulating their interactions with the environment and neighboring organisms. Despite soil biodiversity, NM biotransformation in terrestrial ecosystems has primarily focused on plant-nanomaterial interfaces and several studies have assessed the fate of CeO_2 NMs in the vicinity of plant roots.[5-7] Due to the electronic structure of CeO_2 NMs, the Ce(IV)/Ce(III).

ratio at the NM surface is variable, while the core atoms are mainly in a Ce(IV) state.[8] Partial Ce reduction of CeO_2 NMs was measured in several plant species such as tomato[9], wheat[5] and cucumber[10]. Owing to this versatile redox reactivity, CeO_2 NM is a good candidate to assess the NM biotransformation in soil.

The root surface[6, 9, 11, 12] and root-soil interface[7] are the sites of interaction between plants and NMs. Root metabolites excreted at these interfaces induce a reduction of CeO_2 NMs in plant systems.[6, 13] Plenty of metabolites are candidates (saccharides, amino acids, organic acid, phenols, etc.), yet only citric acid and ascorbic acid were shown to reduce CeO_2 NMs, through incubation experiments simulating root exudates.[11] Soil and root associated bacteria also release a large set of secondary metabolites in their environment for their nutrition (dissolution and uptake of iron, phosphate, etc.), and for their communication with other microorganisms and plants. For instance, biodissolution of Au NMs has been induced by the associated microbiome of a freshwater macrophyte, despite the high chemical stability of Au NMs.[14] The main driver of Au biodissolution is its oxidation and complexation with a secondary metabolite, i.e. cyanide, emitted by microorganisms.[14] Regarding CeO_2 NMs, their transformation by bacteria has been little addressed in the literature and the mechanism is poorly documented. Up to 50% of reduced Ce occur in *Escherichia coli* and *Synechocystis* sp. exposed to 7 nm CeO_2 NMs.[15, 16] However, the soil bacterium *Bacillus subtilis* has proven inefficient in reducing Ce in rod-ceria 8.5 nm x.168 nm NMs, without the addition of exogenous ascorbic acid.[17] The bacterial cell surface is the nano-bio interface that promotes the reduction of CeO_2 NMs,[16,

[17] however the mechanisms and the potential bacterial metabolites allowing this reduction are still unknown.

What are the differences in terms of cell interface and secondary metabolism between bacteria that do (*E. coli* and *Synechocystis* sp., gram-negative bacteria) or do not reduce (*B. subtilis*, gram-positive bacteria) CeO_2 NMs? Apart from the structural differences in their outer envelope, Gram-negative and Gram-positive bacteria differ in the way they metabolize glucose, i.e. a carbon source for bacteria. Both take up glucose and metabolize it by phosphorylation to generate energy-rich molecules (e.g. ATP). However, Gram-negative bacteria can shut down this pathway and enable rapid conversion of glucose to gluconic acid, and then to 2-keto-gluconic acid instead.[18, 19] Gluconic acid and 2-keto-gluconic acid can both be secreted at the outer bacterial membrane surface, and later internalized to feed the cell metabolism. Gluconic acid is the preferred substrate, and is metabolized to pyruvic acid and then citric acid through the Krebs cycle.[20] 2-keto-gluconic acid is a reserve substrate for *Pseudomonas* sp. and known to accumulate in the rhizosphere.[21] This ability to rapidly convert and subtract glucose from other species, and to secrete 2-keto-gluconic acid is a key feature involved in the ecological fitness of Gram-negative bacteria, such as *Pseudomonas* sp., a diverse, ubiquist and ecologically significant soil bacteria. Citric acid and 2-keto-gluconic acid are important metabolites secreted by *Pseudomonas* sp. to solubilize phosphate[22] and chelate iron[23]. As they are released at the cell membrane interface, these two organic acids stand out as two potential metabolite candidates for CeO_2 NM biotransformation.

Key physicochemical properties of NMs, such as their shape, size and surface charge, drive their fate and their biological impact in the environment.[24] Among octahedral, cubic, rod, and irregularly shaped CeO_2-NMs, rod-like particles are transformed to a greater degree than other CeO_2-NMs in solutions simulating plant exudates in hydroponic cucumber plants.[25] According to the particle shape and surface chemistry, CeO_2 NMs exhibits both pro- and antioxidant activities, with the former being toxic to *E. coli* [26]. The surface charge of CeO_2 NMs has been shown to affect Ce(IV) biotransformation with a partial reduction into Ce(III) in activated sludge bioreactors[27], in the nematode *Caenorhabditis elegans*[28], and in wheat[5] and tomato[9]. The size and aggregation of CeO_2 NMs drive the microbial activity and bacterial community structure in the canola rhizosphere.[29] Therefore, the biotransformation of CeO_2 NMs depends on the NM properties but also on the tested organisms and environmental conditions.[28, 30, 31] No marked relation between the size of CeO_2 NMs and the extent of Ce reduction in the organisms has been noted to date.

While predicted concentration of CeO_2 NMs in soils ranges from $ng.kg^{-1}$ to $mg.kg^{-1}$ [32-36], most studies addressing Ce biotransformation used concentrations close to or higher than 100 $mg.kg^{-1}$.[37] One of the reasons for this is the technical difficulty of detecting, quantifying and characterizing CeO_2 NMs at lower concentrations in complex matrices. Recent advances in X-ray absorption spectroscopy (XAS) such as high-energy resolution fluorescence detected XAS (HERFD-XAS) have enabled measurement of XANES spectra with higher energy resolution, i.e. with an apparent core hole lifetime broadening around 0.70eV, smaller than the probed electronic level bandwidth (around 3.2eV) and a lower

detection limit (as low as 60 mg Ce/kg). [38,39] The better defined edge and pre-edge features in the HERFD-XAS spectra enable clear detection of the presence of Ce(III) in the structure of CeO_2-NMs.[39, 40] It is essential to determine the oxidation state of CeO_2 NMs so as to be able to identify the potential biotransformation of CeO_2 NMs, a process which influences their bioavailability and potential ecotoxicity.[13, 41, 42]

This study aimed at identifying the biotransformation mechanisms of different sizes and shapes of CeO_2 NMs by *P. brassicacearum* NFM421, a phytobenefic soil bacteria isolated from *Arabidopsis thaliana* and *Brassica napus* plants.[43] We investigated the fate of CeO_2 NMs in contact with *P. brassicacearum* cells in planktonic conditions, and in cell-free incubations with specific metabolites of citric acid and 2-keto-gluconic acid. Ascorbic acid was also tested as a positive control to assess Ce reduction. The bacterial metabolism and cell growth cycle are interconnected: different sets of metabolites are produced throughout the three growth phases in planktonic conditions. We therefore explored CeO_2 NM reduction by *P. brassicarearum* at different steps of the growth cycle (i.e. the latence phase, where cells adapt to their environment, the exponential phase, where cells divide, and the stationary phase, where cells adapt to the nutrient reduction conditions), and we tested the secretome, i.e. all metabolites excreted by the bacteria in the late exponential phase. We used HERFD-XAS and were thus able to assess changes in Ce speciation and identify the drivers of CeO_2 NMs biotransformation.

Materials and Methods

CeO_2 nanomaterials

Three different sizes of commercially available types of bare CeO_2-NMs were used in this study, all of which are made of cerianite crystallites. Transmission electron microscopy indicated average sizes of 4 nm (CeO_2-4 nm) diameter with a spherical shape (Rhodia Chemicals), 7 nm (CeO_2-7 nm) with an ellipsoidal shape (Rhodia Chemicals), and 31 nm (CeO_2-31 nm) diameter with a spherical shape (Nanograin® Umicore). These NMs have been previously described[16, 29, 30, 39, 44-46] and their characteristics are summarized in the Supporting Information (Table S1). The 7 nm NMs were an ellipsoid of revolution with an average radius of the semi-axes of the ellipsoid of R = 3.5 and 0.91 nm. The specific surface areas were estimated from their size and shape: 231 $m^2.g^{-1}$ for CeO_2-4 nm, 290 $m^2.g^{-1}$ for CeO_2-7 nm and 30 $m^2.g^{-1}$ for CeO_2-31 nm. The surface atom percentages were calculated using the formula given in Deshpande *et al.* [47] using different lattice parameters (0.557 nm 0.553 and 0.547 nm for 4, 7 and 31 nm CeO_2 NMs). We hypothesized that the outer shell of atoms has a finite thickness of half the lattice constant.[47] The percentages of surface atoms were approximately 36%, 41% and 5.2% for the 4 nm, 7 nm and 32 nm forms, respectively).

Bacteria and incubation conditions.

The *Pseudomonas brassicacearum* strain NFM421, a phytobenefic soil-bacteria, was

selected for this study. The *Pseudomonas* genus has a robust metabolism for different carbon sources, and a three-pronged metabolic system to metabolize glucose,[18] a bacterial carbon source that can be released in the rhizosphere from plant roots.[48] The *P. brassicacearum* genome is sequenced, thereby allowing metabolic pathway prediction.[49] Bacterial growth involves three different main phases: i) a lag phase, i.e. a nonreplication period during which the bacterial cells adapt; ii) an exponential phase, during which cell division occurs at a constant rate, with a generation time close to 55 min for *P. brassicacearum*; and iii) the stationary phase, where the growth rate levels off at zero, while the bacteria stay metabolically active and compensate for those that die.

P. brassicacearum NFM421 from frozen stock (−80 °C) was grown at 30°C in 10-fold diluted tryptic soy broth (TSB 1/10) solidified with 15 g L^{-1} agar (Sigma) under dark conditions. After 48 h, a single colony was resuspended in TSB 1/10, incubated overnight at 30°C and stirred at 150 rpm in an orbital shaker, until a concentration of 1×10^9 cells per mL in stationary phase was reached, and this was used as a pre-culture.

Aliquots of the pre-culture were transferred to a new TSB 1/10 medium in order to reach an optical density at 600 nm (OD_{600}) of 0.05 (~ 2.10^6 CFU/mL Figure SI 2). Bacteria and TSB/10 medium were transferred into 50 mL tubes or 1 L erlens, stirred at 150 rpm, incubated until the early exponential growth phase was reached at OD_{600} = 0.1 (~4.10^7 CFU/mL), after approximately 60 min. Several exposures of the *P. brassicacearum* soil bacteria to different sized and shaped CeO_2 NMs were then performed:

1) Exposure to the three sizes of CeO_2 NMs: 4 nm, 7 nm and 31 nm at 5 mg CeO_2/L, from the early- to the late-exponential phase (t3: OD_{600} 0.7 ($2.8\ 10^8$ CFU/mL)). (See SI Figure SI 3).
2) Exposure to several CeO_2-4 nm concentrations: 0.01-0.1-1-5-10 mg CeO_2/L, from the early- to the late-exponential phase (t3). Note that the tested concentration did not affect the bacterial growth.
3) Exposure to CeO_2-7 nm at 5 mg CeO_2/L with bacterial sampling at different times during the exponential phase: t1) OD_{600} 0.15, after 45 min of contact, which was less than the generation time (cell division) for *P. brassicacearum*, t2) OD_{600} 0.3, 90 min mid-exponential phase and t3) OD_{600} 0.7, 165 min, late-exponential phase.

For each size of CeO_2 NMs, a stock solution at 0.3 g Ce/L was prepared prior to bacterial culture dosing. The bacterial culture was incubated at 30°C and stirred at 150 rpm. After the bacterial growth phase, the suspensions were centrifuged at 1500 g at 4°C to separate the bacteria and supernatant. The supernatants were discarded, and the bacterial pellets were either immediately frozen in 5 mm diameter pellets in liquid N_2 and stored at -80°C for XAS measurements, or freeze-dried for ICP-MS analysis.

The effect of the culture medium, single metabolites and secretome (i.e. all metabolites excreted by the bacteria exposed or not to CeO_2 NMs) on the Ce reduction were tested. For these analyses, only CeO_2-4 nm was tested due to time constraints for the Synchrotron analyses and because the extent of bioreduction after bacterial exposure was similar for

4 nm and 7 nm (Figure 1). The culture medium (TSB 1/10) and several commercialized metabolites (2 keto-gluconic acid, ascorbic acid, citric acid from Sigma Aldrich) were incubated with CeO_2-4 nm. The culture medium (TSB 1/10) and citric acid were also incubated with CeO_2-7 nm. Metabolite solutions were prepared at 50 mM concentration, and CeO_2 NMs at 300 mg Ce/L (2 mM) concentration. The metabolites were in excess compared to CeO_2 NMs. Solutions were adjusted to pH=7.2. The suspensions were incubated at 25°C under agitation for 24 h. After the incubation, droplets of the suspensions were frozen in liquid N_2 and kept at -80°C before XAS analyses.

To test the influence on the Ce reduction of the secretome, the bacterial culture supernatant was incubated with CeO_2 NMs. We hypothesized that the bacteria could respond to stress when exposed to NMs responsible for specialized metabolite excretion. We compared two different secretomes: the supernatant of *P. brassicacearum* not exposed to NMs, after a bacterial growth to an OD_{600} of 0.7 (same conditions as explained above), and the supernatant of *P. brassicaceae* exposed to 5 $mg.L^{-1}$ CeO_2-4 nm. After the bacterial growth, the suspensions were centrifuged to separate the bacteria and supernatant. The 4-nm CeO_2 NMs were added to these supernatants at 300 mg Ce/L concentration and incubated under agitation for 24h. After the incubation, droplets of the suspensions were frozen in liquid N_2 and kept at -80°C before the XAS analyses.

ICP MS measurement

The Ce concentration was measured using ICP-MS (PerkinElmer, NexIon 300X) in bacteria exposed to several CeO_2-4 nm concentrations: 0.01-0.1-1-5-10 mg CeO_2/L, from early- to late- exponential phases (t3). Bacterial pellets of three suspensions in 1 L-erlens were pooled to obtain sufficient material for the analysis (30 mg dry weight [DW]), no replicates were performed. Before ICP-MS analysis, each sample was dried and solubilized in acid using a Milestone UltraWAVE® microwave. The acids used for plant sample digestion were 2 mL HNO_3 and 1 mL H_2O_2. The measurement quality was controlled using certified reference materials (mussel tissue BCR-668 from IRMM). All Ce concentrations presented are expressed in mg per kg of dried matter.

XAS measurements

Ce speciation was measured by X-ray absorption near edge structure (XANES) spectroscopy at the European Synchrotron Radiation Facility (ESRF, Grenoble, France). The samples were analyzed in high energy resolution fluorescence detected mode (HERFD) on the FAME-UHD beamline (BM16) using a crystal analyzer spectrometer (CAS) equipped with 5 Ge(331) bent crystals (1 m radius of curvature). With CAS, photons are first optically selected in energy (Bragg diffraction) by the crystals and later collected by a detector, thereby generating a very small energy bandwidth (typically 1-2eV) and thus a higher detection limit and a better spectral resolution.[38, 50] To avoid beam damage, the frozen pellets were analyzed at 10 K using a liquid He cryostat. No photoreduction effect was observed when comparing the different scans. All of the XANES spectra shown here were the sum of 2 to 12 scans, depending on the Ce concentration, in order to

improve the signal-to-noise ratio. Normalization and data reduction were performed using the IFFEFIT software package.[51] Initial CeO_2-NMs, Ce(III)-acetate, Ce(III)-oxalate, Ce(III)-phosphate and Ce(III)-cysteine were used as Ce(IV) and Ce(III) reference samples.

Quantitative determination of the Ce oxidation state was performed through a peak fitting analysis of the pre-edge features of the normalized spectra. To analyze the pre-edge features, a baseline subtraction was first performed by fitting a Gaussian function on the low energy tail of the edge using data a few eV before and after the pre-edge peak.[52, 53] The pre-edges were then deconvoluted into Gaussian components (Pseudo-Voigt was also tested but did not improve the deconvolution performance). As a first step, the Gaussian parameters were allowed to vary for the standard compounds. The Gaussian parameters were then fixed and applied to all spectra (see for example Figure 2C for a deconvolution involving both Ce(III) and Ce(IV)). Two Gaussians functions were used to fit the Ce(III) contribution, with center max positions set at 5718.25 and 5720.87 eV and full widths at half maximum (FWHM) of 2.09 and 1.06 eV, respectively, while the area of each Gaussian function was set at 87% and 13% of the total area, respectively. The Ce(IV) contribution was fitted with one Gaussian with a center max position at 5720.12 eV and an FWHM of 1.77 eV. The pre-edge information was obtained by calculating the "integrated intensity" (sum of the integrated intensities of each component). We hypothesized that the intensity of the pre-edge peak reflects the proportion of the Ce(III) and Ce(IV), however this implies several assumptions. We put forward the hypotheses that: (i) there is a linear relation between the peak integrated area and the Ce oxidation state, (ii) that the local symmetry does not markedly influence the intensity and position of the pre-edge features. It would be difficult to conclude on this last point as the Ce(III) species formed in this study were not identified. To assess the uncertainty of the pre-edge fitting procedure, we calculated theoretical pre-edge spectra for mixtures of Ce(III) and Ce(IV) reference compounds (Ce(III)+Ce(IV)=100% and Ce(III) ranged from 5 to 95%). The peak fitting analysis described above was applied to these mixtures and the relative uncertainty was calculated. The uncertainty ranged from 3 to 22%. The results are thus all expressed with 22% uncertainty and presented as mean ± 0.22*mean.

Results and Discussion

Input of high-energy resolution fluorescence-detected X-ray absorption spectroscopy (HERFD-XAS) for the study of Ce speciation in highly diluted biological samples

Unequivocal identification of the Ce redox state in CeO_2 NMs

XANES at the Ce L3-edge was sensitive to the Ce oxidation state with one intense white line typical of Ce(III) (feature A in Ce(III)-acetate, Figure 1) and two peaks for Ce(IV) (features B and C in CeO_2 NMs, Figure 1) related to the Ce 5d electron density of states.[40] However, feature A, located at 5729 eV, could also be attributed to crystal field splitting

(into e_g and t_{2g}) for Ce(IV) in CeO_2 nanoparticles.[38] With HERFD-XANES, the pre-edge features clearly distinguished the contributions of Ce(III) and Ce(IV) to the signal (Figure 2b). The Ce(III) compound pre-edges showed two features, i.e. D and F, with maximum peaks at 5718 and 5721 eV, respectively, while the Ce(IV) compound pre-edges showed a single peak E with a maximum at 5720 eV. Peaks D and E were easily distinguishable with HERFD-XAS as they were separated by approx. 2eV. Regardless of the NM size, HERFD-XANES analysis solely revealed the presence of the Ce(IV) oxidation state (SI Table 2) in the CeO_2 NMs tested before interaction with bacteria. This result is in agreement with the previously observed absence of Ce(III) inside CeO_2 NMs.[40, 54] Therefore we confirmed the absence of Ce(III) for several sizes of CeO_2 NMs.

Major advance in the speciation of highly diluted Ce bacteria

In this study, we analyzed Ce in bacteria exposed to concentrations as low as 10 µg Ce/L. XAS measurement using CAS allows the study of diluted chemical elements and therefore realistic NM concentrations. The predicted Ce concentration in soil ranged from ng/kg to mg/kg, depending on the area and the soil usage, such as sludge-amended soil or urban soil[32, 36, 55], but no predictions of environmental Ce concentrations in soil solution have been published to date. In aquatic media, the Ce predicted environmental concentration ranged from 1 ng/L to 1 µg/L.[36] With bacterial cell concentrations ranging from 10^4 to 10^6 CFU/mL, thereby representing an NM/cell ratio ranging from 4.8 to 4.8 10^5. In this study, the bacterial density ranged from 4. 10^7 to 2.8 10^8 CFU/mL, and the NM/cell ratio from 1.7 10^2 to 1.2 10^6 depending on the CeO_2 NM concentration exposure. Therefore, the NM/cell ratio tested in this study was very plausible compared to the environmental prediction.

The Ce L3-edge XANES of bacteria exposed to CeO_2-4nm ranged from 0.01 to 10 mg/L, indicating a dominant single absorption edge peak located at 5729 eV, which is typical of Ce(III) (Figure 3). The pre-edge peak analysis confirmed a major Ce(III) contribution of > 70 ± 15% for 5 and 10 mg CeO_2/L concentrations (Table SI 3). The Ce concentrations of these bacteria ranged from 6.2 to 1870 mg Ce/kg DW (Table 1). To date, the lowest Ce concentration analyzed by bulk Ce L3 edge XANES in environmental samples was 35 mg Ce/kg DW.[11] HERFD-XANES analysis therefore improved the detection limit, since XANES were recorded for concentrations as low as 6.2 mg Ce/kg DW. To our knowledge, this is the first time that Ce speciation has been detected at concentrations below 10 mg/kg DW in biological samples. Note that the bacterial samples were analyzed frozen and hydrated (> 90 % water content), therefore with lower exposure Ce concentrations of around 1 mg/kg dried or freeze-dried samples could be used for the analyses.

Size-dependent biotransformation of Ce NMs

The bacterial growth cycle comprises three main phases, each with a specific physiological profile. In the lag phase, just after introduction in the fresh medium, cells sense the environment and retool the machinery in preparation for the exponential phase,

during which they actively divide, depending on the energy sources and nutrients. At the late-exponential phase, as the energy sources are depleted and metabolic waste products accumulate, cells enter in the stationary phase, where growth apparently ceases, with equivalent rates of bacterial cell growth and death. The late exponential phase is an interesting step in the bacterial growth cycle. Secondary metabolism involved in microbial and ecological interactions tends to occur at these late exponential and stationary bacterial growth phases.[56]

The speciation of the Ce accumulated in bacteria after exposure to three different sizes of CeO_2 NMs was measured in the late-exponential phase (Figure 1). We obtained contrasted results between bacteria exposed to 31 nm-spherical CeO_2 NMs and to the two small sizes: 4 nm-spherical and 7 nm-ellipsoidal. XANES spectra of bacteria exposed to 31 nm CeO_2 NMs overlapped the spectra of initial CeO_2 NMs, indicating that the atomic structure of the CeO_2 NMs was not markedly affected. XANES spectra of bacteria exposed to CeO_2-31 nm were fitted with 100% Ce(IV) using Ref 31 nm_CeO_2 (see Table SI 2). XANES spectra of bacteria exposed to 4 nm and 7 nm showed a dominant absorption edge (feature A, Figure 1) typical of the presence of Ce(III). The reduction was similar between the two sizes: pre-edge peak fitting indicated a contribution of Ce(III) of 70 ± 15% for 4 nm CeO_2 NMs and 64 ± 14% for 7 nm CeO_2 NMs at 5 mg Ce/L (Table SI 3). To avoid a potential Ce reduction due to the composition of the culture medium with 1.4 mM K_2HPO_4, CeO_2-4 nm was incubated in sterilized TSB/10 medium for 24 h and no Ce reduction was detected by XAS (Figure 4B). Our results showed that the 4 and 7 nm CeO_2 NMs were biotransformed whereas 31 nm were not modified after bacterial exposure.

Several physicochemical mechanisms could explain the differences in Ce reduction for different CeO_2 NMs, such as aggregation, specific surface area and reactivity.[1, 8, 28, 57] The aggregation state in the media could influence the amount of surface-exposed NMs to bacterial cells. Yan *et al.* suggested that the reduction rates of iron oxide nanoparticles of different sizes (10, 30 and 50 nm) by *Geobacter sulfurreducens* was directly correlated with the bacteria-hematite contact area, while taking NM aggregation into account, not with the total oxide surface area.[58] The isoelectric points (IEP) of CeO_2 NMs, and the pH and ionic strength of the culture media suggested that aggregation could also be expected for the three types of CeO_2 NMs. Since only the 4 and 7 nm CeO_2 NMs were bioreduced, no simple correlation was noted in this study between the aggregation state and the reduction rate.

The Ce(IV) reduction could also be attributed to the redox cycle occurring at the surface of the solid and/or to reductive dissolution.[59] The percentage of surface atoms for the 31-nm NMs was around 5% (Table SI1), whereas the uncertainty of the HERDF-XAS method was ± 22%. This could explain why Ce(III) was not detected at the surface of 31 nm CeO_2 NMs. For the 4 nm and 7 nm CeO_2 NMs, the percentage of Ce(IV) reduction (> 64±14%, Table SI3) was higher than that of surface atoms (>36 %, Table SI1). We suggest that this reduction could be explained by reductive dissolution. Indeed, Ce(III) has high solubility,

with logKs = -21.5 for Ce(III) oxide (Smith, 2004), and its release rate could be expected to exponentially increase as the grain size decreases.[31, 60] To conclude, we hypothesized that the absence, or low Ce reduction, for the 31 nm NMs could be explained by a low reductive dissolution rate due to a lower percentage of surface atoms compared to NMs of under 7 nm.

Biotransformation kinetics

Metabolism is dependent on the phase of the growth cycle. Different sets of metabolites are produced in the primary metabolism, related to cell growth and division *vs.* the secondary metabolism, in the late-exponential and the stationary phases, related to ecological function.[56] To determine the metabolic context in which Ce reduction takes place, we investigated the NM biotransformation kinetics by sampling cells after different exposure times to CeO_2-4 nm and CeO_2-7 nm, from the early-exponential to the stationary phase. Figure 2 shows that for each tested exposure time, a dominant post-absorption edge peak at 5729 eV, characteristic of Ce(III), was observed on all XANES, after exposure to CeO_2-7 nm. The pre-edge peak fitting analysis indicated similar results for all exposure times: 68 ± 15% Ce(III) after 45 and 90 min and 64 ± 14% Ce(III) after 320 min in bacteria exposed to 7 nm CeO_2 (Table SI3). Similar results were obtained after exposure to CeO_2-4 nm: 76 ± 17% Ce(III) after 45 min and 70 ± 15% after 90 and 320 min (Table SI3). Therefore, these results indicated that a partial reduction occurred rapidly (in less than 45 min) in the early-exponential phase and did not vary up to the stationary phase. Interestingly, the conversion of glucose to gluconic acid and to 2-keto-gluconic acid by *Pseudomonas* occurred from the lag to the early exponential phases, which suggests a potential role of these metabolites in the reduction of CeO_2 NMs.

Secretome and interaction between bacteria and NMs

The secretome, i.e. the culture medium sampled after bacterial growth, including all the metabolites excreted by the bacteria, was isolated from the bacterial culture. Figure 4B shows XANES spectra of CeO_2-4 nm incubated in the bacterial secretome, sampled from a control or from a CeO_2-4 nm exposure sample. The spectra were similar between the NM suspension and after incubation in the two scenarios. The pre-edge analysis confirmed the absence of a Ce(III) contribution (Table SI 3). The secretome therefore did not induce a Ce reduction after incubation with NMs. This indicates that the NM/bacterial interaction is needed to induce a Ce reduction. CeO_2 NMs can be adsorbed at the surface of the bacteria, as shown with *Escherischia coli* in the studies of Thill et al. [16] and Zeyons et al.[15]. In the close vicinity of the bacteria, the chemical composition of the media was highly influenced by the bacterial exudation. Locally, the metabolite concentration was much higher than in the sampled secretome. Moreover, the metabolites could also be rapidly degraded in the media. Therefore, the bacterial metabolites in the secretome may not have induced a Ce reduction due to the low concentrations in the media and probable biodegradation.

Reduction of CeO_2 NMs is driven by 2-keto-gluconic acid and citric acid bacterial metabolites

To test the involvement of individual metabolites secreted in the extracellular medium in the Ce reduction, we focused on environmentally relevant metabolites that are known to be secreted in soil, especially in the rhizosphere, as *P. brassicacearum* NFN 421 is a good plant root colonizer.[43] We selected 2-keto-gluconic acid and citric acid bacterial metabolites as potential sources of Ce reduction. As mentioned, these organic acids are produced by *Pseudomonas* sp., and more generally by Gram-negative bacteria, in their environment so as to retrieve phosphate, iron and interact with plants. *P. brassicacearum* contains all the genes necessary for the production and secretion of these metabolites [49]. 2-keto-gluconic acid can be detected in the culture medium of *P. brassicacearum* in the early exponential phase (C. Santaella, personal communication).

CeO_2 NMs were incubated with 2-keto-gluconic acid, citric acid and ascorbic acid (which is not produced by bacteria), as ceria NMs can undergo a reduction with the assistance of these organic acids.[11, 17] All of the tested metabolites induced a partial reduction of CeO_2-4 nm after 24h exposure (Figure 4A). Peak fitting of the pre-edge confirmed the presence of Ce(III) in these samples with 23 ± 5% for citric acid, 30 ± 7% for 2-keto-gluconic acid and 26 ± 6% for ascorbic acid for CeO_2-4 nm, and 31 ± 7 % for ascorbic acid for CeO_2-7 nm (Table SI 4). Note that the bacterial metabolite 2-keto-gluconic acid proved to be as efficient as ascorbic acid, the main plant metabolite currently found to be involved in CeO_2 NMs reduction. As *Pseudomonas* species are ubiquituous bacteria that are frequently present in hydroponic plant cultures, and in the rhizosphere, this suggests the involvement of 2-keto-gluconic acid in CeO_2 NM reduction at the plant root interface. Around 36% of Ce atoms are localized at the surface of CeO_2-4 nm, and 41% for the CeO_2-7 nm. Assuming that the Ce reduction only occurred at the surface, the reductions induced by 2-keto-gluconic acid, citric acid and ascorbic acid for CeO_2-4 nm were 83 ± 19%, 65 ± 14% and 72 ± 17% of the surface atoms. For the CeO_2-7 nm, ascorbic acid induced a reduction of 75 ± 17% in the surface atoms. The metabolites alone, when present in excess in the suspension, were thus able to induce a marked reduction in CeO_2 NMs of the surface atoms. The reduction measured with the tested metabolites remained lower than in the biotic interaction. This could be explained by the implication of other metabolites not tested in this study and the effect of the colocalization of NMs and metabolites at the nano-cell interface.

Overall, our results showed that the biotransformation and fate of NMs was size-dependent, and metabolites such as citric acid and 2-keto-gluconic acid proved efficient in reducing Ce from CeO_2-4 nm. Many soil bacteria other than *Pseudomonas* sp. can secrete 2-keto-gluconic acid,[61] e.g. *Gluconobacter oxidans.* This suggests that in environmentally relevant conditions, the presence of soil microbiota associated with plant roots could contribute to the reduction of CeO_2 NMs. This biotransformation will affect the fate of Ce in the soil and the effect of Ce on soil biota (e.g. bacteria, fungi, macroorganisms and plants).

Beyond the fate of NMs in soil, this is an important result to take into consideration for diverse NM applications because the main properties of CeO_2 NMs will be impacted by biotransformation. For example, it is often speculated that CeO_2 NMs present an autoregenerative mechanisms of valence reversion, thereby explaining the catalytic properties.[41] Interesting, their ability to self-regenerate their surface has biomedical applications.[42] However, if NMs are transformed or if the reduction is total, as observed in our study, it is more than likely that Ce(III) would be released from CeO_2 NMs, thereby making the valence reversion impossible in NMs. Note that *Pseudomonas* sp. also include human pathogens such as *P. aeruginosa* or *P. putida*. Studies using CeO_2 NMs should therefore investigate possible contact of NMs with bacteria and adapt the NM size to take both the modification of NM properties and their environmental fate into account.

Supporting Information: Physicochemical characteristics of nanomaterials; Correlation between the optical density at 600 nm and colony forming units; *Pseudomonas brassicacearum* growth curve; Normalized Ce L_3-edge HERFD-XANES of CeO_2-4 nm, CeO_2-7 nm, CeO_2-31 nm and zoom on the pre-edge region; Pre-peak fitting parameters of the standard compounds; Results of the pre-peak fitting of the samples.

Acknowledgements

The authors thank ESRF for providing beam time access on FAME-UHD/BM16 (experiment EV-202). The FAME-UHD project is financially supported by the French *Grand Emprunt* EquipEx (EcoX, ANR-10-EQPX-27-01), the CEA-CNRS CRG consortium and the INSU CNRS Institute. This work is also a contribution to the OSU-Institut Pythéas. The authors thank CNRS for the IRP iNOVE funding.

1. Lowry, G. V.; Gregory, K. B.; Apte, S. C.; Lead, J. R., Transformations of Nanomaterials in the Environment. *Environ. Sci. Technol.* **2012,** *46*, (13), 6893-6899.
2. Peijnenburg, W. J. G. M.; Baalousha, M.; Chen, J.; Chaudry, Q.; Von der kammer, F.; Kuhlbusch, T. A. J.; Lead, J.; Nickel, C.; Quik, J. T. K.; Renker, M.; Wang, Z.; Koelmans, A. A., A Review of the Properties and Processes Determining the Fate of Engineered Nanomaterials in the Aquatic Environment. *Critical Reviews in Environmental Science and Technology* **2015,** *45*, (19), 2084-2134.
3. Sun, T. Y.; Bornhöft, N. A.; Hungerbühler, K.; Nowack, B., Dynamic Probabilistic Modeling of Environmental Emissions of Engineered Nanomaterials. *Environ. Sci. Technol.* **2016,** *50*, (9), 4701-4711.
4. Wang, Y.; Nowack, B., Dynamic probabilistic material flow analysis of nano-SiO2, nano iron oxides, nano-CeO2, nano-Al2O3, and quantum dots in seven European regions. *Environ. Pollut.* **2018,** *235*, 589-601.
5. Spielman-Sun, E.; Lombi, E.; Donner, E.; Howard, D.; Unrine, J. M.; Lowry, G. V., Impact of Surface Charge on Cerium Oxide Nanoparticle Uptake and Translocation by Wheat (Triticum aestivum). *Environ. Sci. Technol.* **2017,** *51*, (13), 7361-7368.
6. Ma, Y.; Zhang, P.; Zhang, Z.; He, X.; Zhang, J.; Ding, Y.; Zhang, J.; Zheng, L.; Guo, Z.; Zhang, L.; Chai, Z.; Zhao, Y., Where Does the Transformation of Precipitated Ceria Nanoparticles in Hydroponic Plants Take Place? *Environ. Sci. Technol.* **2015,** *49*, (17), 10667-10674.
7. Rico, C. M.; Johnson, M. G.; Marcus, M. A., Cerium oxide nanoparticles transformation at the root–soil interface of barley (Hordeum vulgare L.). *Environmental Science: Nano* **2018,** *5*, (8), 1807-1812.
8. Reed, K.; Cormack, A.; Kulkarni, A.; Mayton, M.; Sayle, D.; Klaessig, F.; Stadler, B., Exploring the properties and applications of nanoceria: is there still plenty of room at the bottom? *Environmental Science: Nano* **2014,** *1*, (5), 390-405.
9. Li, J.; Tappero, R. V.; Acerbo, A. S.; Yan, H.; Chu, Y.; Lowry, G. V.; Unrine, J. M., Effect of CeO2 nanomaterial surface functional groups on tissue and subcellular distribution of Ce in tomato (Solanum lycopersicum). *Environmental Science: Nano* **2019,** *6*, (1), 273-285.
10. Ma, Y. H.; Zhang, P.; Zhang, Z. Y.; He, X.; Li, Y. Y.; Zhang, J.; Zheng, L. R.; Chu, S. Q.; Yang, K.; Zhao, Y. L.; Chai, Z. F., Origin of the different phytotoxicity and biotransformation of cerium and lanthanum oxide nanoparticles in cucumber. *Nanotoxicology* **2015,** *9*, (2), 262-270.
11. Zhang, P.; Ma, Y.; Zhang, Z.; He, X.; Zhang, J.; Guo, Z.; Tai, R.; Zhao, Y.; Chai, Z., Biotransformation of Ceria Nanoparticles in Cucumber Plants. *ACS Nano* **2012,** *6*, (11), 9943-9950.
12. Ma, Y.; Zhang, P.; Zhang, Z.; He, X.; Li, Y.; Zhang, J.; Zheng, L.; Chu, S.; Yang, K.; Zhao, Y.; Chai, Z., Origin of the different phytotoxicity and biotransformation of cerium and lanthanum oxide nanoparticles in cucumber. *Nanotoxicology* **2015,** *9*, (2), 262-70.
13. Zhang, W. L.; Dan, Y. B.; Shi, H. L.; Ma, X. M., Elucidating the mechanisms for plant uptake and in-planta speciation of cerium in radish (Raphanus sativus L.) treated with cerium oxide nanoparticles. *J. Environ. Chem. Eng.* **2017,** *5*, (1), 572-577.
14. Avellan, A.; Simonin, M.; McGivney, E.; Bossa, N.; Spielman-Sun, E.; Rocca, J. D.; Bernhardt, E. S.; Geitner, N. K.; Unrine, J. M.; Wiesner, M. R., Gold nanoparticle biodissolution by a freshwater macrophyte and its associated microbiome. *Nature Nanotechnology* **2018,** *13*, (11), 1072-1077.

15. Zeyons, O.; Thill, A.; Chauvat, F.; Menguy, N.; Cassier-Chauvat, C.; Orear, C.; Daraspe, J.; Auffan, M.; Rose, J.; Spalla, O., Direct and indirect CeO2 nanoparticles toxicity for Escherichia coli and Synechocystis. *Nanotoxicology* **2009,** *3*, (4), 284-295.
16. Thill, A.; Zeyons, O.; Spalla, O.; Chauvat, F.; Rose, J.; Auffan, M.; Flank, A. M., Cytotoxicity of CeO2 nanoparticles for Escherichia coli. Physico-chemical insight of the cytotoxicity mechanism. *Environ. Sci. Technol.* **2006,** *40*, (19), 6151-6156.
17. Xie, C.; Zhang, J.; Ma, Y.; Ding, Y.; Zhang, P.; Zheng, L.; Chai, Z.; Zhao, Y.; Zhang, Z.; He, X., Bacillus subtilis causes dissolution of ceria nanoparticles at the nano–bio interface. *Environmental Science: Nano* **2019,** *6*, (1), 216-223.
18. Udaondo, Z.; Ramos, J. L.; Segura, A.; Krell, T.; Daddaoua, A., Regulation of carbohydrate degradation pathways in Pseudomonas involves a versatile set of transcriptional regulators. *Microbial biotechnology* **2018,** *11*, (3), 442-454.
19. Sun, W.; Alexander, T.; Man, Z.; Xiao, F.; Cui, F.; Qi, X., Enhancing 2-Ketogluconate Production of Pseudomonas plecoglossicida JUIM01 by Maintaining the Carbon Catabolite Repression of 2-Ketogluconate Metabolism. *Molecules* **2018,** *23*, (10).
20. Daddaoua, A.; Krell, T.; Alfonso, C.; Morel, B.; Ramos, J.-L., Compartmentalized Glucose Metabolism in Pseudomonas putida Is Controlled by the PtxS Repressor. *Journal of Bacteriology* **2010,** *192*, (17), 4357-4366.
21. Moghimi, A.; Tate, M.; Oades, J., Characterization of rhizosphere products especially 2-ketogluconic acid. *Soil Biology and Biochemistry* **1978,** *10*, (4), 283-287.
22. Vyas, P.; Gulati, A., Organic acid production in vitro and plant growth promotion in maize under controlled environment by phosphate-solubilizing fluorescent Pseudomonas. *BMC Microbiology* **2009,** *9*, (1), 174.
23. Buch, A. D.; Archana, G.; Kumar, G. N., Enhanced citric acid biosynthesis in Pseudomonas fluorescens ATCC 13525 by overexpression of the Escherichia coli citrate synthase gene. *Microbiology (Reading, England)* **2009,** *155*, (8), 2620-2629.
24. Auffan, M.; Bottero, J.-Y.; Chaneac, C.; Rose, J., Inorganic manufactured nanoparticles: how their physicochemical properties influence their biological effects in aqueous environments. *Nanomedicine* **2010,** *5*, (6), 999-1007.
25. Zhang, P.; Xie, C.; Ma, Y.; He, X.; Zhang, Z.; Ding, Y.; Zheng, L.; Zhang, J., Shape-dependent transformation and translocation of ceria nanoparticles in cucumber plants. *Environmental Science & Technology Letters* **2017,** *4*, (9), 380-385.
26. Damle, M. A.; Jakhade, A. P.; Chikate, R. C., Modulating Pro- and Antioxidant Activities of Nanoengineered Cerium Dioxide Nanoparticles against Escherichia coli. *ACS Omega* **2019,** *4*, (2), 3761-3771.
27. Barton, L. E.; Auffan, M.; Bertrand, M.; Barakat, M.; Santaella, C.; Masion, A.; Borschneck, D.; Olivi, L.; Roche, N.; Wiesner, M. R.; Bottero, J. Y., Transformation of Pristine and Citrate-Functionalized CeO2 Nanoparticles in a Laboratory-Scale Activated Sludge Reactor. *Environ. Sci. Technol.* **2014,** *48*, (13), 7289-7296.
28. Collin, B.; Oostveen, E.; Tsyusko, O. V.; Unrine, J. M., Influence of Natural Organic Matter and Surface Charge on the Toxicity and Bioaccumulation of Functionalized Ceria Nanoparticles in Caenorhabditis elegans. *Environ. Sci. Technol.* **2014,** *48*, (2), 1280-1289.
29. Hamidat, M.; Barakat, M.; Ortet, P.; Chaneac, C.; Rose, J.; Bottero, J.-Y.; Heulin, t.; Achouak, W.; Santaella, C., Design defines the effects of nanoceria at a low dose on soil microbiota and the potentiation of impacts by canola plant. *Environ. Sci. Technol.* **2016,** *50*, (13), 6892-6901.
30. Tella, M.; Auffan, M.; Brousset, L.; Issartel, J.; Kieffer, I.; Pailles, C.; Morel, E.; Santaella, C.; Angeletti, B.; Artells, E.; Rose, J.; Thiery, A.; Bottero, J. Y., Transfer,

Transformation, and Impacts of Ceria Nanomaterials in Aquatic Mesocosms Simulating a Pond Ecosystem. *Environ. Sci. Technol.* **2014,** *48*, (16), 9004-9013.
31. Misra, S. K.; Dybowska, A.; Berhanu, D.; Luoma, S. N.; Valsami-Jones, E., The complexity of nanoparticle dissolution and its importance in nanotoxicological studies. *Science of The Total Environment* **2012,** *438*, 225-232.
32. Park, B.; Donaldson, K.; Duffin, R.; Tran, L.; Kelly, F.; Mudway, I.; Morin, J. P.; Guest, R.; Jenkinson, P.; Samaras, Z.; Giannouli, M.; Kouridis, H.; Martin, P., Hazard and risk assessment of a nanoparticulate cerium oxide-based diesel fuel additive - A case study. *Inhal. Toxicol.* **2008,** *20*, (6), 547-566.
33. Johnson, A. C.; Park, B., Predicting contamination by the fuel additive cerium oxide engineered nanoparticles within the United Kingdom and the associated risks. *Environ Toxicol Chem* **2012,** *31*, (11), 2582-7.
34. Gottschalk, F.; Lassen, C.; Kjoelholt, J.; Christensen, F.; Nowack, B., Modeling Flows and Concentrations of Nine Engineered Nanomaterials in the Danish Environment. *International Journal of Environmental Research and Public Health* **2015,** *12*, (5), 5581.
35. Meesters, J. A. J.; Quik, J. T. K.; Koelmans, A. A.; Hendriks, A. J.; van de Meent, D., Multimedia environmental fate and speciation of engineered nanoparticles: a probabilistic modeling approach. *Environmental Science: Nano* **2016,** *3*, (4), 715-727.
36. Giese, B.; Klaessig, F.; Park, B.; Kaegi, R.; Steinfeldt, M.; Wigger, H.; von Gleich, A.; Gottschalk, F., Risks, Release and Concentrations of Engineered Nanomaterial in the Environment. *Scientific Reports* **2018,** *8*, (1), 1565.
37. Layet, C.; Auffan, M.; Santaella, C.; Chevassus-Rosset, C.; Montes, M.; Ortet, P.; Barakat, M.; Collin, B.; Legros, S.; Bravin, M. N.; Angeletti, B.; Kieffer, I.; Proux, O.; Hazemann, J.-L.; Doelsch, E., Evidence that Soil Properties and Organic Coating Drive the Phytoavailability of Cerium Oxide Nanoparticles. *Environ. Sci. Technol.* **2017,** *51*, (17), 9756-9764.
38. Proux, O.; Lahera, E.; Del Net, W.; Kieffer, I.; Rovezzi, M.; Testemale, D.; Irar, M.; Thomas, S.; Aguilar-Tapia, A.; Bazarkina, E. F.; Prat, A.; Tella, M.; Auffan, M.; Rose, J.; Hazemann, J.-L., High-Energy Resolution Fluorescence Detected X-Ray Absorption Spectroscopy: A Powerful New Structural Tool in Environmental Biogeochemistry Sciences. *J. Environ. Qual.* **2017,** *46*, (6), 1146-1157.
39. Tella, M.; Auffan, M.; Brousset, L.; Morel, E.; Proux, O.; Chaneac, C.; Angeletti, B.; Pailles, C.; Artells, E.; Santaella, C.; Rose, J.; Thiery, A.; Bottero, J. Y., Chronic dosing of a simulated pond ecosystem in indoor aquatic mesocosms: fate and transport of CeO2 nanoparticles. *Environmental Science: Nano* **2015,** *2*, (6), 653-663.
40. Cafun, J. D.; Kvashnina, K. O.; Casals, E.; Puntes, V. F.; Glatzel, P., Absence of Ce3+ Sites in Chemically Active Colloidal Ceria Nanoparticles. *ACS Nano* **2013,** *7*, (12), 10726-10732.
41. Pulido-Reyes, G.; Rodea-Palomares, I.; Das, S.; Sakthivel, T. S.; Leganes, F.; Rosal, R.; Seal, S.; Fernandez-Pinas, F., Untangling the biological effects of cerium oxide nanoparticles: the role of surface valence states. *Sci Rep* **2015,** *5*, 15613.
42. Rajeshkumar, S.; Naik, P., Synthesis and biomedical applications of cerium oxide nanoparticles–a review. *Biotechnology Reports* **2018,** *17*, 1-5.
43. Achouak, W.; Sutra, L.; Heulin, T.; Meyer, J.-M.; Fromin, N.; Degraeve, S.; Christen, R.; Gardan, L., Pseudomonas brassicacearum sp. nov. and Pseudomonas thivervalensis sp. nov., two root-associated bacteria isolated from Brassica napus and Arabidopsis thaliana. *International Journal of Systematic and Evolutionary Microbiology* **2000,** *50*, (1), 9-18.

44. Auffan, M.; Tella, M.; Santaella, C.; Brousset, L.; Paillès, C.; Barakat, M.; Espinasse, B.; Artells, E.; Issartel, J.; Masion, A., An adaptable mesocosm platform for performing integrated assessments of nanomaterial risk in complex environmental systems. *Scientific reports* **2014,** *4*, (1), 5608.
45. Auffan, M.; Rose, J.; Orsiere, T.; De Meo, M.; Thill, A.; Zeyons, O.; Proux, O.; Masion, A.; Chaurand, P.; Spalla, O.; Botta, A.; Wiesner, M. R.; Bottero, J. Y., CeO2 nanoparticles induce DNA damage towards human dermal fibroblasts in vitro. *Nanotoxicology* **2009,** *3*, (2), 161-U115.
46. Nabavi, M.; Spalla, O.; Cabane, B., Surface Chemistry of Nanometric Ceria Particles in Aqueous Dispersions. *Journal of Colloid and Interface Science* **1993,** *160*, (2), 459-471.
47. Deshpande, S.; Patil, S.; Kuchibhatla, S.; Seal, S., Size dependency variation in lattice parameter and valency states in nanocrystalline cerium oxide. *Applied Physics Letters* **2005,** *87*, (13), 3.
48. Stubbs, V.; Standing, D.; Knox, O.; Killham, K.; Bengough, A.; Griffiths, B., Root border cells take up and release glucose-C. *Annals of Botany* **2004,** *93*, (2), 221-224.
49. Ortet, P.; Barakat, M.; Lalaouna, D.; Fochesato, S.; Barbe, V.; Vacherie, B.; Santaella, C.; Heulin, T.; Achouak, W., Complete genome sequence of a beneficial plant root-associated bacterium, Pseudomonas brassicacearum. **2011,** *193*, (12), 3146-3146.
50. Llorens, I.; Lahera, E.; Delnet, W.; Proux, O.; Braillard, A.; Hazemann, J. L.; Prat, A.; Testemale, D.; Dermigny, Q.; Gelebart, F.; Morand, M.; Shukla, A.; Bardou, N.; Ulrich, O.; Arnaud, S.; Berar, J. F.; Boudet, N.; Caillot, B.; Chaurand, P.; Rose, J.; Doelsch, E.; Martin, P.; Solari, P. L., High energy resolution five-crystal spectrometer for high quality fluorescence and absorption measurements on an x-ray absorption spectroscopy beamline. *Review of Scientific Instruments* **2012,** *83*, (6), 9.
51. Ravel, B.; Newville, M., ATHENA, ARTEMIS, HEPHAESTUS: data analysis for X-ray absorption spectroscopy using IFEFFIT. *J Synchrotron Radiat* **2005,** *12*, (Pt 4), 537-41.
52. Bordage, A.; Balan, E.; de Villiers, J. P.; Cromarty, R.; Juhin, A.; Carvallo, C.; Calas, G.; Raju, P. S.; Glatzel, P., V oxidation state in Fe–Ti oxides by high-energy resolution fluorescence-detected X-ray absorption spectroscopy. *Physics and Chemistry of Minerals* **2011,** *38*, (6), 449-458.
53. Wilke, M.; Farges, F.; Petit, P.-E.; Brown Jr, G. E.; Martin, F., Oxidation state and coordination of Fe in minerals: An Fe K-XANES spectroscopic study. *American Mineralogist* **2001,** *86*, (5-6), 714-730.
54. Plakhova, T. V.; Romanchuk, A. Y.; Butorin, S. M.; Konyukhova, A. D.; Egorov, A. V.; Shiryaev, A. A.; Baranchikov, A. E.; Dorovatovskii, P. V.; Huthwelker, T.; Gerber, E.; Bauters, S.; Sozarukova, M. M.; Scheinost, A. C.; Ivanov, V. K.; Kalmykov, S. N.; Kvashnina, K. O., Towards the surface hydroxyl species in CeO2 nanoparticles. *Nanoscale* **2019,** *11*, (39), 18142-18149.
55. Liu, H. H.; Cohen, Y., Multimedia Environmental Distribution of Engineered Nanomaterials. *Environ. Sci. Technol.* **2014,** *48*, (6), 3281-3292.
56. O'Brien, J.; Wright, G. D., An ecological perspective of microbial secondary metabolism. *Current opinion in biotechnology* **2011,** *22*, (4), 552-558.
57. Collin, B.; Auffan, M.; Johnson, A. C.; Kaur, I.; Keller, A. A.; Lazareva, A.; Lead, J. R.; Ma, X.; Merrifield, R. C.; Svendsen, C.; White, J. C.; Unrine, J. M., Environmental release, fate and ecotoxicological effects of manufactured ceria nanomaterials. *Environmental Science: Nano* **2014,** *1*, (6), 533-548.
58. Yan, B.; Wrenn, B. A.; Basak, S.; Biswas, P.; Giammar, D. E., Microbial Reduction of Fe(III) in Hematite Nanoparticles by Geobacter sulfurreducens. *Environ. Sci. Technol.* **2008,** *42*, (17), 6526-6531.

59. Schwabe, F.; Schulin, R.; Rupper, P.; Rotzetter, A.; Stark, W.; Nowack, B., Dissolution and transformation of cerium oxide nanoparticles in plant growth media. *Journal of Nanoparticle Research* **2014,** *16*, (10), 2668.
60. Adamson, A. W.; Gast, A. P., *Physical Chemistry of Surfaces, 6th Edition*. Interscience publishers New York: 1997; Vol. 150, p 808.
61. Hou, Z.; Sun, L.; Wang, D.; Sun, W.; Cui, F.; Yu, S., Production of 2-keto-gluconic acid from glucose by immobilized Pseudomonas plecoglossicida resting cells. *3 Biotech* **2020,** *10*, (6), 253.

Figures :

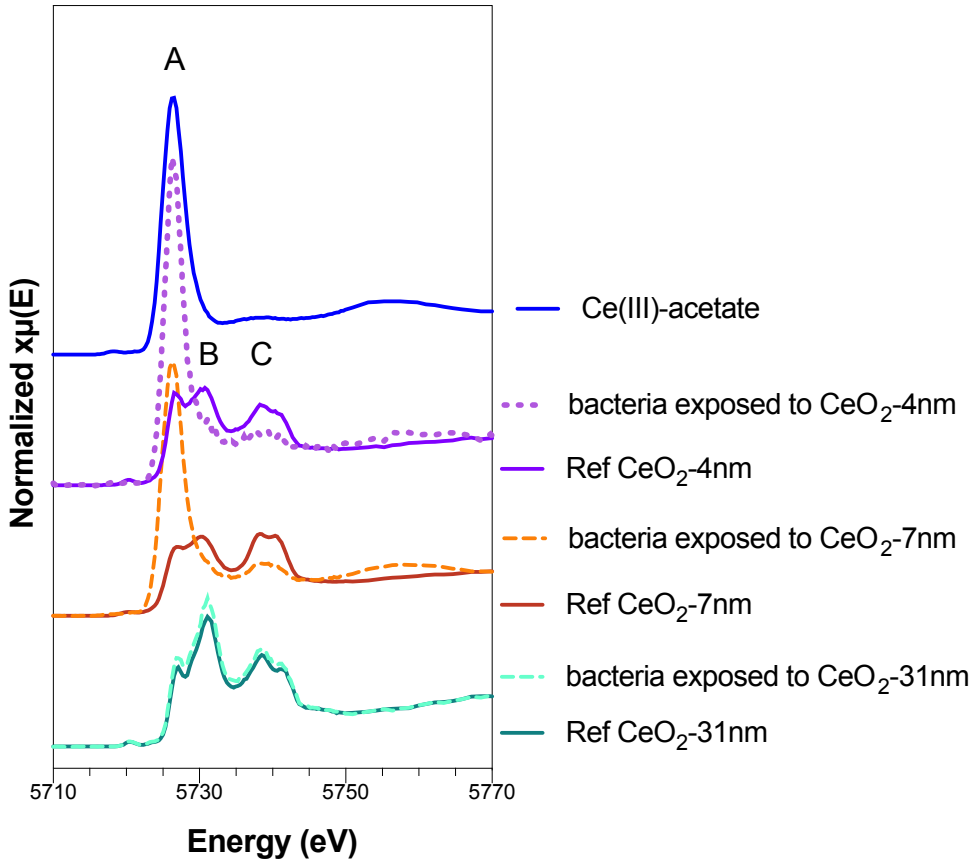

Figure 1 - Normalized Ce L_3-edge high energy resolution fluorescence detected (HERFD) XANES of *Pseudomonas brassicacearum* exposed to three different sizes of nanomaterials (NMs): 4 nm, 7 nm and 31 nm CeO_2 at 5 mg $Ce.L^{-1}$. Ce(III)–acetate, and the initial CeO_2-NMs Ce(IV) are shown as reference compounds (BM13, ESRF). Bacteria were sampled at an optical density at 600 nm (OD_{600}) of 0.7 (320 min exposure). Spectra of bacteria exposed to CeO_2-7 nm are the same as the spectra t3 (OD_{600} 0.7) 320 min in Figure 2. Feature A, located at 5729 eV, indicated a characteristic features of Ce(III) and features B and C characteristic features of Ce(IV). However, feature A, could also be attributed to crystal field splitting (into eg and t2g) for Ce(IV) in CeO_2 NMs.

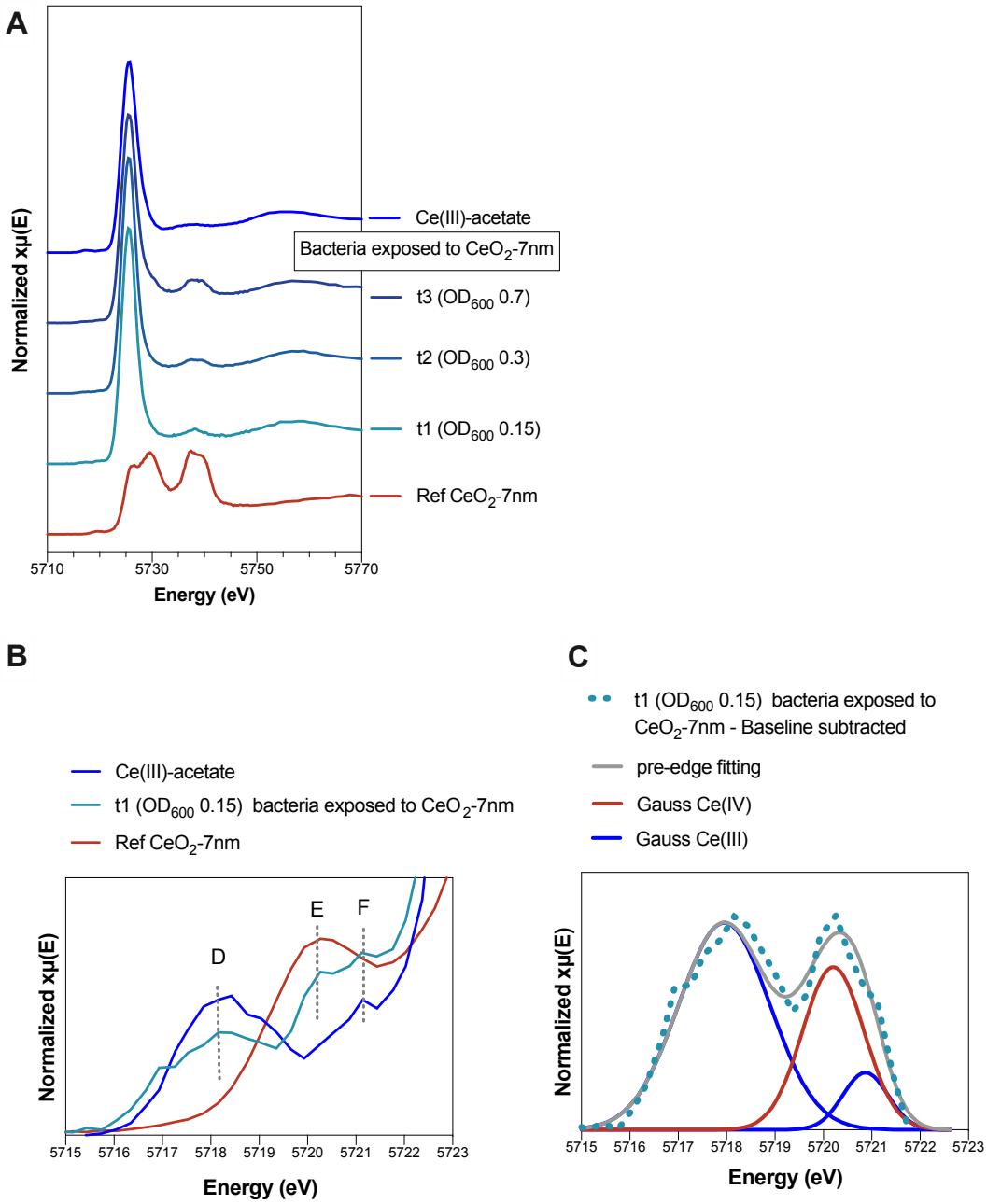

Figure 2 – A) Normalized Ce L_3-edge high energy resolution fluorescence detected (HERFD) XANES of *Pseudomonas brassicacearum* exposed to CeO_2-7 nm at 5 mg $Ce.L^{-1}$ for several incubation times: t1 (OD_{600} 0.15) 45 min, t2 (OD_{600} 0.3) 90 min, t3 (OD_{600} 0.7) 320 min . Ce(III)–acetate, and the CeO_2-7 nm are shown as reference compounds (BM13, ESRF). Spectra t3 (OD_{600} 0.7) are the same as the spectra shown in Figure 1 of bacteria exposed to CeO_2-7 nm. B) Zoom of the pre-edge region for the reference compound and *Pseudomonas brassicacearum* exposed to CeO_2-7 nm at 5 mg $Ce.L^{-1}$ for 45 min t1 (OD_{600} 0.15). The Ce(III) compound pre-edges showed two features, i.e. D and F, with maximum peaks at 5718 and 5721 eV, respectively, while the Ce(IV) compound pre-edges showed a single peak E with a maximum at 5720 eV. C) Extracted pre-edge of *Pseudomonas brassicacearum* exposed to CeO_2-7 nm at 5 mg $Ce.L^{-1}$ for 45 min t1 (OD600 0.15) and the corresponding pre-edge peak fitting after baseline subtraction. Two Gaussian functions fitted the Ce(III) and one fitted the Ce(IV).

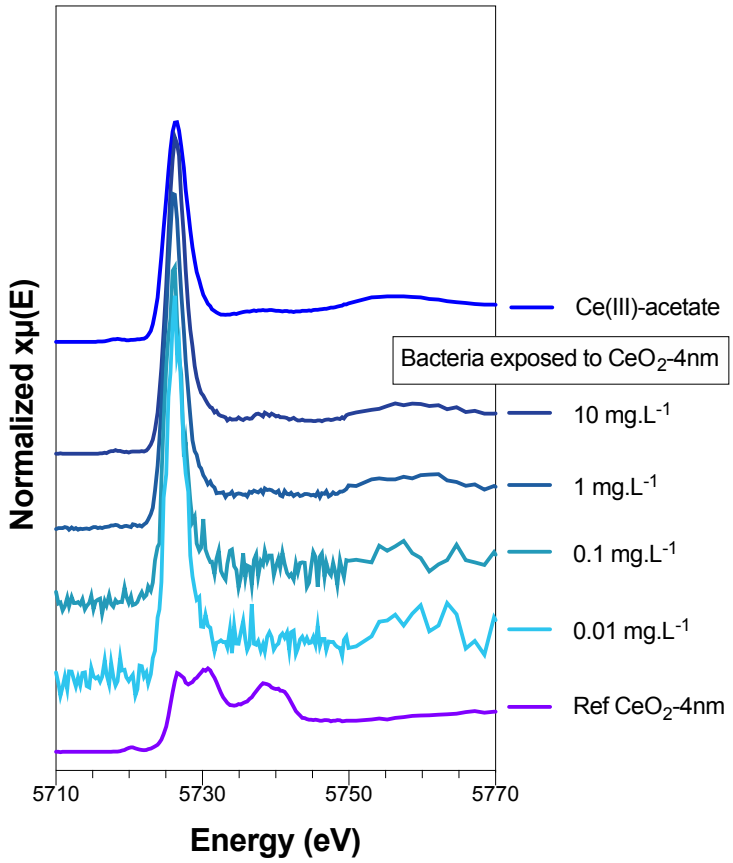

Figure 3 - Normalized Ce L_3-edge high energy resolution fluorescence detected (HERFD) XANES of *Pseudomonas brassicacearum* exposed to CeO_2-4 nm at several concentrations from 0.01 to 10 mg Ce .L^{-1}. Ce(III)–acetate, and the initial CeO_2 NMs are shown as reference compounds (BM13, ESRF).

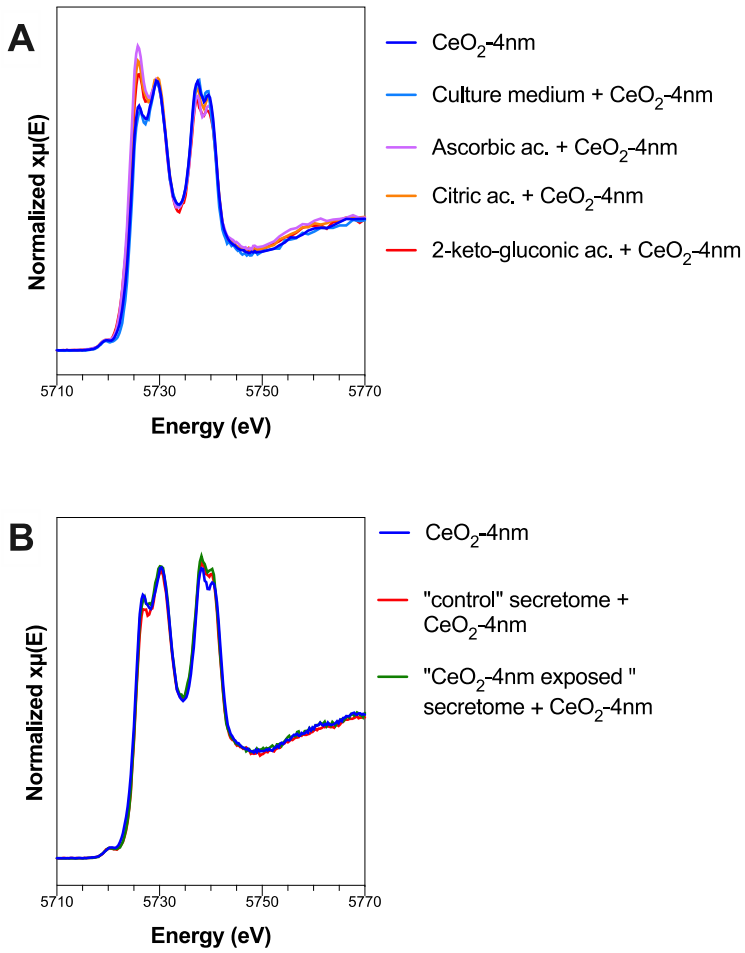

Figure 4 - Normalized Ce L_3-edge high energy resolution fluorescence detected (HERFD) XANES of CeO_2-4 nm and different incubations (A) incubations of CeO_2-4 nm with the growth culture medium (TSB1/10) and several metabolites: ascorbic acid, citric acid, 2-keto-gluconic acid (B) incubations of CeO_2-4 nm NMs with the secretome: culture medium (TSB1/10) after 24 h of *Pseudomonas brassicacearum* growth, exposed or not to CeO_2-4 nm during growth.

Table 1: Ce concentration (mg.kg^{-1} dry weigh) in bacteria *Pseudomonas brassicacearum* exposed at several CeO_2-4 nm concentrations from the early- to late- exponential phase nanoparticles OD_{600} 0.7 (2.8 10^8 CFU/mL).

CeO_2 concentration in exposure medium (mg.L^{-1})	Ce concentration in bacteria (mg.kg^{-1} DW)
0.01	6.2
0.1	43
1	382
5	1196
10	1872